Advances in Radiation Oncology (2025) **10**, 101681

advances in radiation oncology

www.advancesradonc.org

Scientific Article

Comprehensive Image Quality Evaluation and Motion Phantom Studies of an Ultra-Fast (6-Second) Cone-Beam Computed Tomography Imaging System on a Ring Gantry Linear Accelerator

Hui Zhao, PhD,[a,*] Geoff Nelson, PhD,[a] Vikren Sarkar, PhD,[a] Courtney Oare, PhD,[b] Martin Szegedi,[a] Sara St. James, PhD,[a] Jeremy Kunz, PhD,[a] Ryan Price, PhD,[a] and Y. Jessica Huang, PhD[a]

[a]Department of Radiation Oncology, University of Utah, Salt Lake City, Utah; and [b]Department of Radiation Oncology, University of Minnesota, Minnesota

Received 16 November 2023; accepted 4 November 2024

Purpose: To evaluate the image quality of an ultrafast cone-beam computed tomography (CBCT) system—Varian HyperSight.

Methods and Materials: In this evaluation, 5 studies were performed to assess the image quality of HyperSight CBCT. First, a HyperSight CBCT image quality evaluation was performed and compared with Siemens simulation-CT and Varian TrueBeam CBCT. Second, a visual comparison of image quality among simulation-CTs, HyperSight CBCT, and TrueBeam CBCT was performed for a patient with head and neck cancer and patients with metal dental fillings and prostheses. Third, the Hounsfield unit (HU) versus electron density curve of HyperSight CBCT was compared with GE and Siemens simulation CTs. Fourth, Siemens simulation-CT and HyperSight CBCT scans were acquired on the Catphan set-up at different locations inside the bore (±10 cm in all 3 principal directions from the center), and the HU variations for different materials were evaluated. Fifth, a 4-dimensional lung tumor phantom study was performed to assess moving tumor alignment during image registration.

Results: Significant improvement of image contrast, HU constancy, and noise level on HyperSight CBCT was observed compared with TrueBeam CBCT. Significant image quality improvement was observed on HyperSight CBCT for patients with dental fillings and prostheses compared with simulation-CT without metal artifact reduction. The linear fit trendline of HU versus electron density curves for GE simulation-CT, Siemens simulation-CT, and HyperSight CBCT showed a 0.6% difference for HU values below 2000. The maximum HU difference for HyperSight CBCT when Catphan was positioned within ±10 cm in all 3 principal directions was ≤ 98 on bone 50%, ≤ 29 other than bone, and was ≤ 31 on bone 50%, and ≤ 17 other than bone for Siemens simulation-CT. Both tumor shape and tumor alignment discrepancies on CBCT scans were observed in a 4-dimensional phantom study.

Conclusions: This evaluation shows significant image improvement of HyperSight CBCT over conventional CBCT on image contrast, HU constancy, and noise level with scatter correction and metal artifact reduction reconstruction methods. HyperSight CBCT has similar image quality to simulation-CTs and shows the potential application for treatment planning. The rapid acquisition of HyperSight CBCT showed both tumor shape and tumor alignment discrepancies of moving targets. Careful considerations of patient respiratory motion monitoring and target matching are highly recommended.

Sources of support: This work had no specific funding.

Research data are stored in an institutional repository and will be shared upon request to the corresponding author.

*Corresponding author: Hui Zhao, PhD, DABR; Email: hui.zhao@hci.utah.edu

https://doi.org/10.1016/j.adro.2024.101681

Introduction

Cone-beam (CB) computed tomography (CT) (CBCT) has been applied as an effective image-guided radiation therapy (IGRT) modality caused by the convenience of scan acquisition from its integration with linear accelerator treatment machines and 3-dimensional (3D) volumetric patient anatomy assessment. However, native CBCT scans acquired from most current commercially available IGRT imaging systems suffer noticeable imaging noise and artifacts caused by photon scatter and metal objects in the scan area, as well as inaccurate and inconsistent Hounsfield unit (HU) values.[1-4] These deficiencies limit the accuracy of IGRT image registration and the potential of adaptive radiation therapy (RT) using CBCT for treatment planning. To improve CBCT image quality, investigations of further scatter correction and metal artifact reduction on original CBCT have been performed using various technologies, and the image quality of postprocessed CBCT has been improved to certain degrees to be able to perform better IGRT image registration and enable adaptive RT.[1-11]

The HyperSight (Varian Medical Systems) equipped Halcyon ring gantry linear accelerator is a newly US Food and Drug Administration-cleared imaging system with 2 new iterative CBCT reconstruction methods, scatter correction (iCBCT Acuros) and metal artifact reduction (iCBCT MAR) in 2023. The image panel for HyperSight is enlarged to 86 × 43 cm compared with 40 × 30 cm for the Varian C-arm imaging system. This unique combination of an enlarged image panel, advanced detector hardware, and improved reconstruction algorithms has enabled HyperSight to achieve a full-fan acquisition with a half-arc (211°) rotation in just 5.9 seconds. Several previous Halcyon CBCT imaging studies were performed based on the older version Halcyon system with an acquisition time of 17 to 42 seconds.[12,13] Additionally, a recent study comparing image quality among HyperSight CBCT, Varian TrueBeam CBCT, and fan-bean simulation-CT on patients was published.[14] The results from Robar et al[14] showed significant artifact reduction on HyperSight CBCT compared with TrueBeam CBCT and comparable image artifacts between HyperSight CBCT and fan-beam simulation-CT. The median HU for HyperSight breath hold imaging was within 15 HU compared to simulation-CT.

The advancements in CBCT technology in recent years have allowed effective imaging registration for accurate treatments using IGRT, including for moving targets such as lung and liver tumors.[15-19] However, there are potential concerns with using 3D free-breathing CBCT,[20-24] such as image artifacts caused by motion, changes in target motion magnitude, uncertainty of tumor location, significant loss of volumetric information, and localization errors caused by underestimated internal target volume (ITV). Some of these issues can be addressed using HyperSight CBCT with a rapid 5.9-second scanning time. Given the normal human respiratory rate of 12 to 18 breaths per minute, this 5.9-second scanning time corresponds to approximately only 1 to 1.5 respiratory cycles. The ultrafast HyperSight CBCT has the potential to significantly reduce motion artifacts. However, such a rapid image acquisition may also cause tumor alignment discrepancy between simulation-CT and CBCT scans of moving targets, depending on the motion amplitude, motion speed, and motion phase during CBCT acquisition.[25,26] In this study, the tumor alignment during image registration of rapid HyperSight CBCT with simulation-CT of a moving lung tumor was evaluated.

With its newly US Food and Drug Administration-cleared status, reports of both general and comprehensive image quality evaluation of the HyperSight system are currently limited. The goals of this evaluation are to answer 3 questions:

1. Does HyperSight CBCT show significant image improvement over conventional CBCT on image quality?
2. Is the image quality of HyperSight CBCT adequate for treatment planning, compared with simulation-CT?
3. Does the rapid CBCT scan of HyperSight cause misalignment of the moving target?

Materials and Methods

A new HyperSight-equipped Halcyon linear accelerator (version 4.0) was installed in our clinic in February 2023. There were 2 simulation CTs in our clinic, a Siemens SOMATOM Confidence (Siemens Healthineers) and a GE LightSpeed RT16 (GE Health Care). The GE simulation CT was decommissioned around the time when the Halcyon was installed; therefore, there was some variation of data availabilities between different simulation CTs. HyperSight CBCT on Halcyon provides full fan acquisition with 4-kilovolt settings: 80, 100, 125, and 140 kV, and 4 different CBCT reconstruction methods: standard, iCBCT, iCBCT Acuros (scatter correction), and iCBCT MAR (metal artifact reduction). The normal field of view (FOV) range for CBCT is 28.2 to 53.8 cm. In this evaluation, 5 studies were performed to assess the image quality of HyperSight CBCT.

First, a detailed HyperSight CBCT image quality evaluation was performed on a phantom (Catphan, model 604, Phantomlab); all CT image quality was analyzed using the TotalQA system (Image Owl). In this section, 2 analytic matrices were used to evaluate the HyperSight CBCT image quality:

1. Image quality for each combination of the four kV settings with four different CBCT reconstruction methods was assessed.
2. An image quality comparison between HyperSight CBCT, Siemens simulation-CT, and Varian TrueBeam CBCT (version 2.7.4) was conducted.

Because of default values and configuration limitations on different imaging systems, we used the following parameters to compile this study. The HyperSight CBCT scans can only be acquired using a full fan. The TrueBeam CBCT scans for 80 and 100 kV were acquired using a full fan, and for 125 and 140 kV were acquired using a half fan by default (not customizable). The FOV of all HyperSight CBCT scans was 28.2 cm—the narrowest FOV allowed on the Halcyon for the best image quality. The FOV for Siemens simulation-CT was adjusted to 28.2 cm for proper comparison. The kilovolt settings for Siemens simulation-CT were 80, 100, 120, and 140 kV; a 125 kV setting is not available. The FOV of TrueBeam CBCT for 80 and 100 kV was 26.2 cm, which was not adjustable on the TrueBeam machine. The FOV of TrueBeam CBCT with standard reconstruction for 125 and 140 kV was adjusted to 28.2 cm to match HyperSight CBCT, and the FOV of TrueBeam CBCT with iCBCT reconstruction was 46.5 cm, which was also not adjustable. The image quality of HyperSight CBCT with the widest FOV (53.8 cm) for a combination of all kilovolt settings and reconstruction methods was also analyzed.

Second, a visual comparison of the image quality among GE simulation-CT, HyperSight CBCT, and TrueBeam CBCT was performed on patient scans.

1. For a patient with head and neck cancer.
2. For 10 patients with metal dental fillings and 5 patients with prostheses.

Third, the HU versus electron density curve was assessed among HyperSight CBCT, GE simulation-CT, and Siemens simulation-CT.

1. The HyperSight CBCT scan was acquired on an Advanced Electron Density Phantom (Sun Nuclear). All standard inserts (physical density from 0.29 to 1.93 g/cm^3) were placed inside the phantom.[27] Detailed information on the phantom can be found on the Sun Nuclear website: https://www.sunnuclear.com/products/advanced-electron-density-phantom.
2. The HU versus electron density curve was generated for HyperSight CBCT and compared with the ones for the GE simulation-CT and Siemens simulation-CT. The region of interest used for generating the curve was created to cover the inserts as large as possible but not to exceed the outer layer of the inserts. The volume of the region of interest was 47 cc for most inserts and 37 cc for the true water inserts to exclude the air bubbles inside the inserts.

Fourth, both Siemens simulation-CT and HyperSight CBCT scans of the Catphan were acquired with the phantom at different locations within the bore (center, 10 cm left, 10 cm right, 10 cm anterior, 10 cm posterior, 10 cm superior, and 10 cm inferior from the center), and the HU variation for different materials was evaluated and compared.

Fifth, a 4-dimensional (4D) lung tumor phantom study was performed.

1. A 4D simulation-CT scan was acquired using Siemens simulation-CT on a Computerized Imaging Reference Systems (CIRS) phantom (008A Dynamic Phantom, Sun Nuclear), in which a 2 cm spherical tumor was programmed to move sinusoidally in the superior-inferior direction with ± 5 mm amplitude with a 6-second cycle. The kilovolt setting for the scan was 120 kV, the slice thickness was 2 mm, and the reconstruction method was filtered back-projection.
2. The ITV of the tumor was contoured using the average intensity projection (AIP) data set derived from 4D CT, and the AIP data set was used as a reference for image registration. Figure 1A shows a screenshot of the AIP data set with the ITV contour.
3. Sixty-nine HyperSight CBCT scans were acquired using a combination of different tumor motion amplitudes (± 2 mm, ± 5 mm, ± 7 mm, ± 10 mm), motion cycle times (1-12 seconds in 1-second increment), and the CBCT acquisition coinciding with different phases of the tumor motion (inhalation, exhalation, both inhalation, and exhalation). In this study, inhalation was defined as superior motion and exhalation was defined as inferior motion.
4. Offline image registration was performed to align the entire phantom, and the final alignment of the ITV was evaluated.
5. Tumor alignments for all CBCT scans were grouped and summarized into several scenarios, including:
   - Tumor motion within ± 5 mm with motion cycle ≤ 6 seconds
   - Tumor motion amplitude of ± 5 mm and slower motion cycle (6-12 seconds)
   - Tumor motion amplitudes exceeding ± 5 mm with motion cycle ≤ 6 seconds
   - Tumor motion amplitude exceeding ± 5 mm and motion period exceeding 6 seconds.

Results

Table 1 shows a comparison of basic image quality among HyperSight CBCT, Siemens simulation-CT, and Varian TrueBeam CBCT in our clinic. For iCBCT Acuros and iCBCT MAR, with 125 and 140 kV settings, a significant improvement of image contrast, HU constancy, and

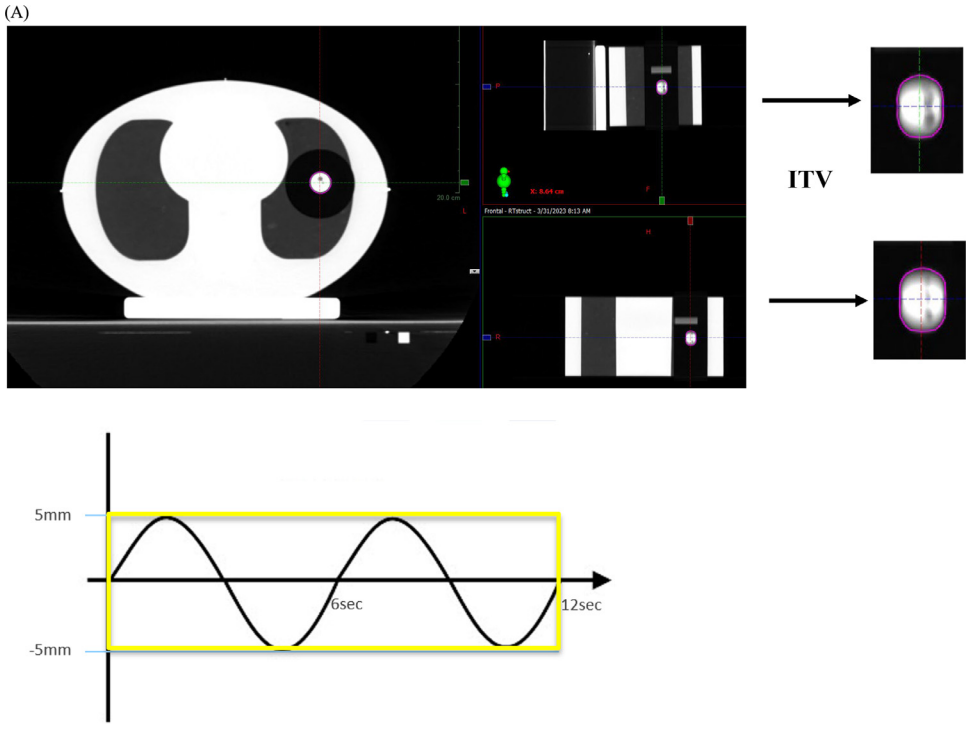

Figure 1 (A) Average intensity projection (AIP) image on a CIRS phantom showing a 2 cm spherical lung tumor with ± 5 mm superior-inferior sinusoidal motion with a 6-second cycle and computed tomography (CT) acquisition time encompassing the entire respiratory cycle (yellow-boxed area). (B) HyperSight cone-beam CT (CBCT) in a combination of ± 5 mm motion amplitude with 1-second (top) and 6-second (bottom) motion cycle rate. For a 1-second motion cycle rate, the CBCT acquisition time encompasses 6 breathing cycles. (C) HyperSight CBCT in combination with ± 5 mm tumor motion amplitude, 12-second motion cycle rate, and CBCT acquisition time encompassing the entire inhalation phase (yellow-boxed area). (D) HyperSight CBCT in a combination of ± 10 mm tumor motion amplitude with a 6-second motion cycle rate. (E) HyperSight CBCT in combination with different tumor motion amplitude, motion cycle rate, and the motion phase of CBCT acquisition.
Abbreviations: ITV = internal target volume.

noise level on HyperSight CBCT over TrueBeam is shown in the table. With similar image contrast achieved, HU constancy and noise level for HyperSight CBCT were slightly superior to Siemens simulation-CT with 125 and 140 kV settings for iCBCT Acuros and ICBCT MAR. The image quality of iterative reconstruction with 125 and 140 kV settings was highlighted (bold fonts) for comparison because Varian released treatment planning capability on HyperSight CBCT with iCBCT Acuros and iCBCT MAR for 125 and 140 kV. The image quality parameters of HyperSight CBCT with the widest FOV (53.8 cm) were similar to the FOV of 28.2 cm, with the exception of the spatial resolution in the range between 4 and 5 lp/cm caused by the larger FOV. Both CT dose index and milliampere-seconds for all scans were listed in Table 2. The CT dose index for each CBCT scan was provided as a parameter by HyperSight, which correlated to the CBCT scanning protocol, including kilovolts and milliampere seconds.

In reviewing images from different modalities across sixteen cases involving various body sites, both with and without metal implants, we observed that HyperSight CBCT demonstrated comparable, if not superior, image quality based on user feedback at our institution. Figures 2-5 provide imaging examples that illustrate these findings. Figure 2 shows the image quality comparison among simulation-CT, HyperSight CBCT, and TrueBeam CBCT on the same patient with head and neck cancer treated in our clinic. This patient was originally treated on TrueBeam and was then transferred to Halcyon. There was observably less noise and better contrast in the HyperSight CBCT compared to TrueBeam CBCT, and the visual image quality of HyperSight CBCT was similar to the fan-beam simulation CT. Figure 3 illustrates the image quality comparison between GE simulation-CT, Siemens simulation-CT, and HyperSight CBCT on patients with metal dental fillings. Figure 3A compares a Siemens simulation-CT with metal artifact reduction to a HyperSight CBCT with iCBCT MAR. Figure 3B compares a GE simulation-CT to a HyperSight CBCT with iCBCT MAR. Our GE CT machine was not capable of metal artifact reduction. A significant improvement in image quality was observed on the HyperSight CBCT MAR compared with GE simulation-CT (which was obvious because GE CT did not have a metal artifact reduction function) for 2 patients included in our study. It was

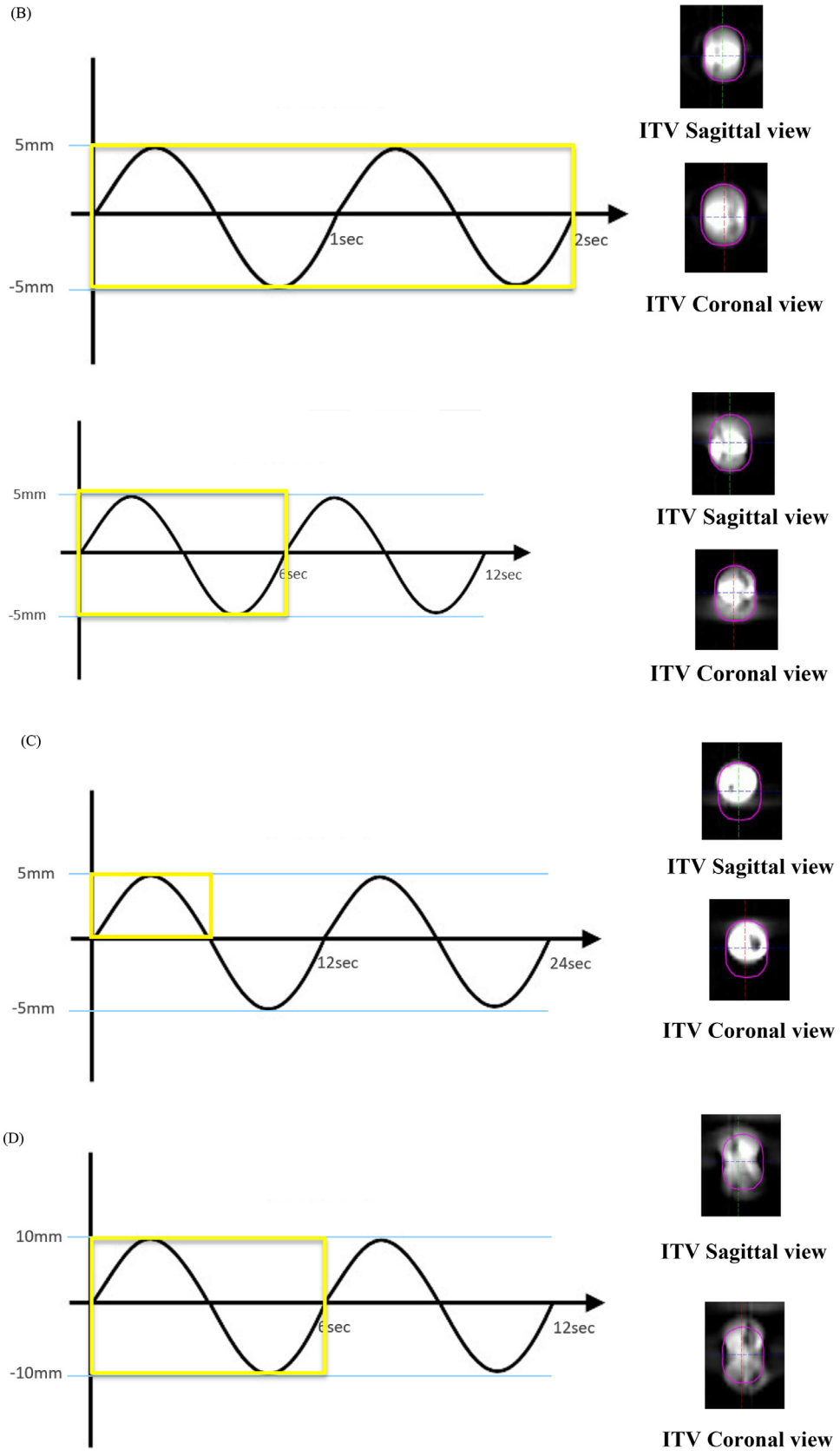

Figure 1 **Continued.**

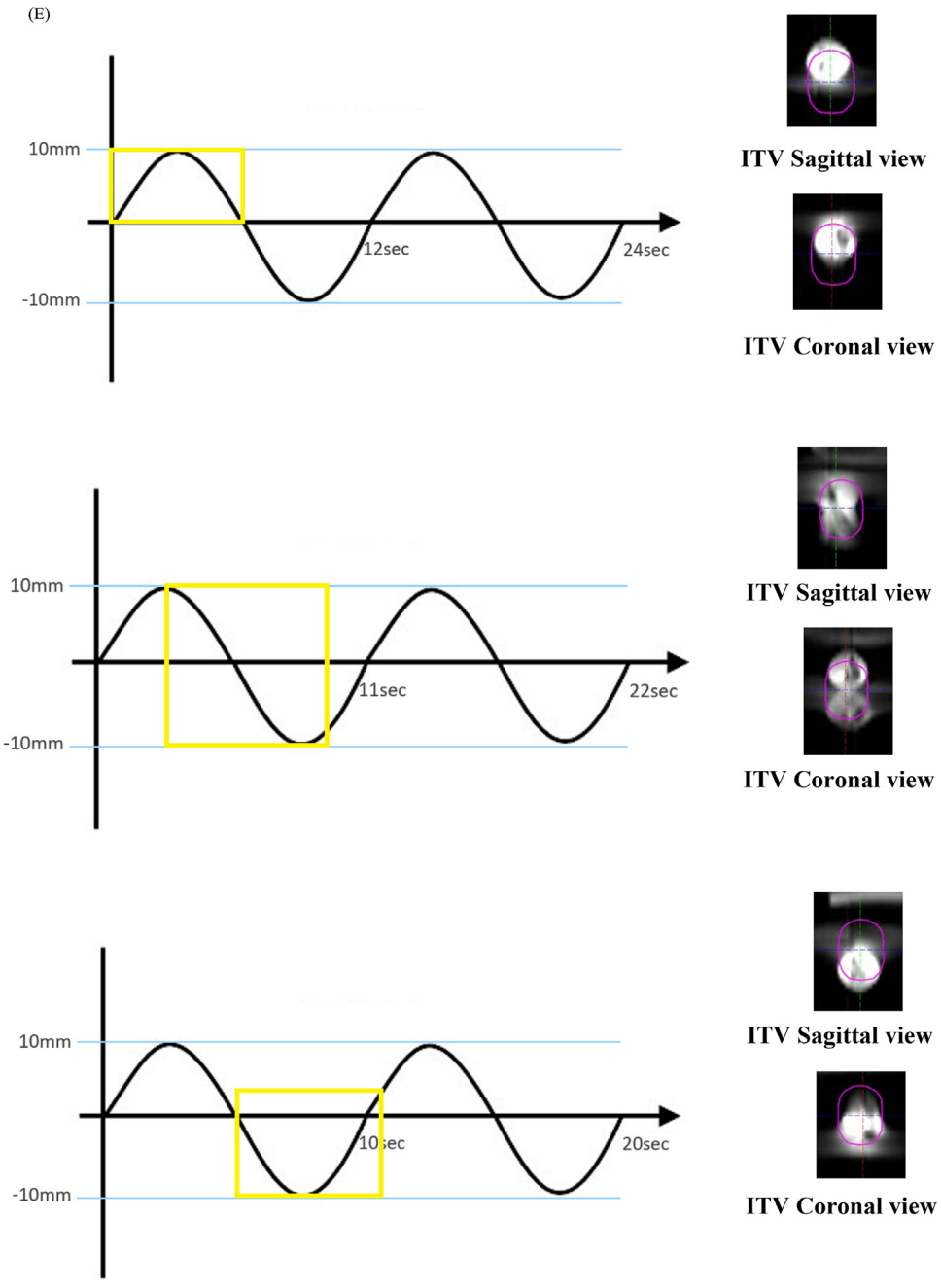

Figure 1 **Continued.**

also observed that similar image quality on the HyperSight CBCT MAR compared with Siemens simulation-CT MAR for the rest 8 patients. Figure 4 shows another example of the image quality comparison between GE simulation-CT and HyperSight CBCT on a patient with a prosthetic hip. Significant improvements in image quality were visually observed on the HyperSight CBCT MAR for all 5 patients with prosthetic hips.

Figure 5 shows the HU versus electron density curve comparison among GE simulation-CT, Siemens simulation-CT, and HyperSight CBCT in our clinic. The linear fit trendline of the 3 curves showed a 0.6% difference for HU values below 2000, which was the maximum measured HU value.

The HU consistency for HyperSight CBCT scans with iCBCT Acuros reconstruction is shown in Table 3, when Catphan was in different positions inside the Halcyon bore within ± 10 cm in all 3 principal directions. The maximum HU difference for 125 kV was 98 and for 140 kV was 90, both on bone 50%. The maximum HU difference for both 125 and 140 kV was ≤ 29 other than bone (50% and 20%). The HU consistency for Siemens

Table 1 Comparison of basic image quality among Halcyon HyperSight CBCT (FOV 28.2 cm), Siemens simulation-CT, and TrueBeam CBCT

		HyperSight CBCT reconstruction method			Siemens CT	TrueBeam	
kV setting	CBCT Quality	Standard FDK	iCBCT Acuros	iCBCT MAR	Iterative	Standard	iCBCT
80	Geometry distortion (mm)	0.02	0.03	0.04	0.03	0.06	0.07
	Spatial resolution (lp/cm)	6.81	6.86	7.02	5.06	7	6.44
	Contrast (1% level) (mm)*	9	9	9	5	15	15
	HU constancy (HU)	18	34	34	19	3	22
	Uniformity (HU)	24.6	23.8	19.6	2.4	31.4	29.0
	Noise (HU)	44.0	30.9	31.7	16.2	67.9	42.2
100	Geometry distortion (mm)	0.01	0.04	0.02	0.01	0.09	0.13
	Spatial resolution (lp/cm)	6.85	6.61	7.31	6.38	7.05	7.04
	Contrast (1% level) (mm)	8	7	6	4	8	8
	HU constancy (HU)	17	5	17	22	19	17
	Uniformity (HU)	20.5	14.1	16.4	0.9	6.3	6.8
	Noise (HU)	23.2	15.5	15.4	10.4	33.2	15.8
125	Geometry distortion (mm)	0.03	**0.00**	**0.02**	**0**	0.03	**0.08**
	Spatial resolution (lp/cm)	6.92	**6.61**	**6.43**	**6.39**	5.89	**4.25**
	Contrast (1% level) (mm)	3	**3**	**2**	**3**	9	**8**
	HU constancy (HU)	14	**4**	**1**	**23**	18	**17**
	Uniformity (HU)	22.2	**14.6**	**13.3**	**1.9**	21.5	**12.9**
	Noise (HU)	7.7	**6.1**	**4.5**	**7.9**	19.7	**8.1**
140	Geometry distortion (mm)	0.00	**0.03**	**0.01**	**0.00**	0.08	**0.08**
	Spatial resolution (lp/cm)	6.9	**6.64**	**6.42**	**5.94**	6.35	**4.37**
	Contrast (1% level) (mm)	3	**2**	**2**	**3**	5	**NA****
	HU constancy (HU)	12	**3**	**3**	**23**	25	**11**
	Uniformity (HU)	21.2	**13.0**	**15.0**	**2.2**	24.5	**20.3**
	Noise (HU)	5.3	**3.1**	**2.9**	**6.7**	20.4	**20.3**

Contrast (1% level).

Abbreviations: CT = computed tomography; CBCT = cone-beam computed tomography; FOV = normal field of view; HU = Hounsfield unit.

mm*: the diameter of the smallest detectable region of interest.[26]

NA**: not detectable.

The image metrics definition can be found on below ImageOwl website: https://help.imageowl.com/hc/en-us/articles/360017635673-CBCT-CT-Catphan-Phantom.

The image quality of iterative reconstruction with 125 and 140 kV settings was highlighted (bold fonts) for comparison because Varian released treatment planning capability on HyperSight CBCT with iCBCT Acuros and iCBCT MAR for 125 and 140 kV.

Table 2 Comparison of CTDI and mAs among Halcyon HyperSight CBCT (FOV 28.2 cm), Siemens simulation-CT, and TrueBeam CBCT in image quality tests

	HyperSight CBCT		Siemens CT		TrueBeam CBCT	
kV setting	CTDI (mGy)	mAs	CTDI (mGy)	mAs	CTDI (mGy)	mAs
80	1.1	100	2.04	83	0.94	100
100	3.87	167	4.18	86	3.17	150
125	9.95	523	7.66	92	15.35	1038
140	25.75	1000	10.96	91	36.58	1678

Abbreviations: CT = computed tomography; CBCT = cone-beam computed tomography; CTDI = CT dose index; FOV = normal field of view.

simulation-CT scans with iterative reconstruction is shown in Table 4 when Catphan was in different positions inside the bore. The Catphan could only be moved down a maximum of 9 cm from the center to ensure couch clearance. The maximum HU difference for both 120 and 140 kV was ≤ 31, on bone 50%, and was ≤ 17 on other than bone (50% and 20%). No HU variations for superior/inferior position were tested for Siemens simulation-CT because the CT scans were helical. The lowest and highest HU numbers in each category are highlighted. The HU range for each material provided in the Catphan 604 manual is also listed in the table.

In the 4D lung tumor phantom study, several scenarios were observed. The overall results of the 4D lung tumor phantom study are summarized in Table 5.

1. For tumor motion within ±5mm and motion cycle ≤ 6 seconds, the agreement between the center of the tumor on HyperSight CBCT and the center of ITV position on the AIP reference image was observed, as shown in Fig. 1B. The tumor shape shown on CBCT was similar to AIP—a solid center with surrounded motion blur.

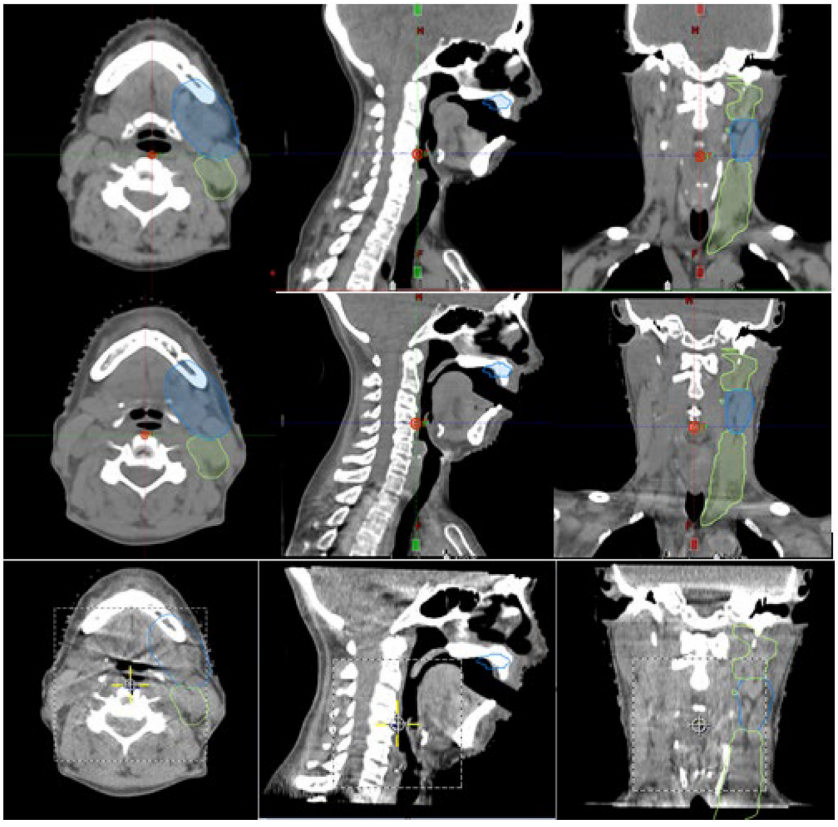

Figure 2 Comparison of GE simulation-computed tomography (CT), HyperSight cone-beam (CB) CT, and TrueBeam CBCT for the same patient. The top figures were fan-beam GE simulation-CT, the middle figures were HyperSight CBCT with iCBCT Acuros reconstruction, and the bottom figures were TrueBeam CBCT with standard reconstruction.

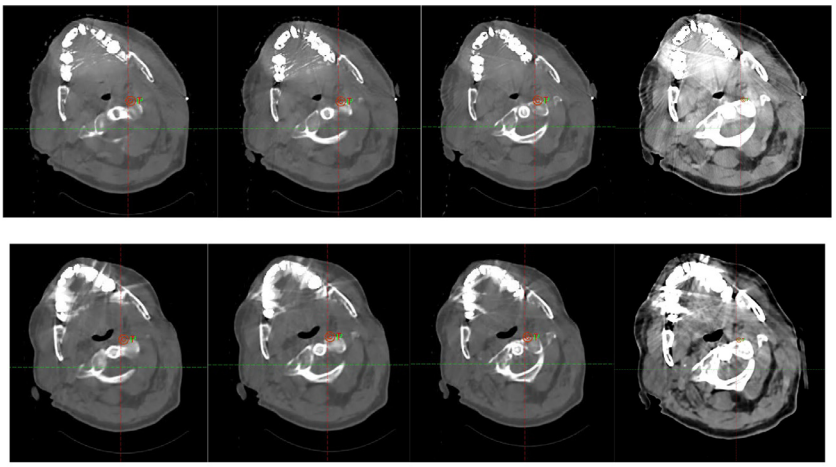

(A)

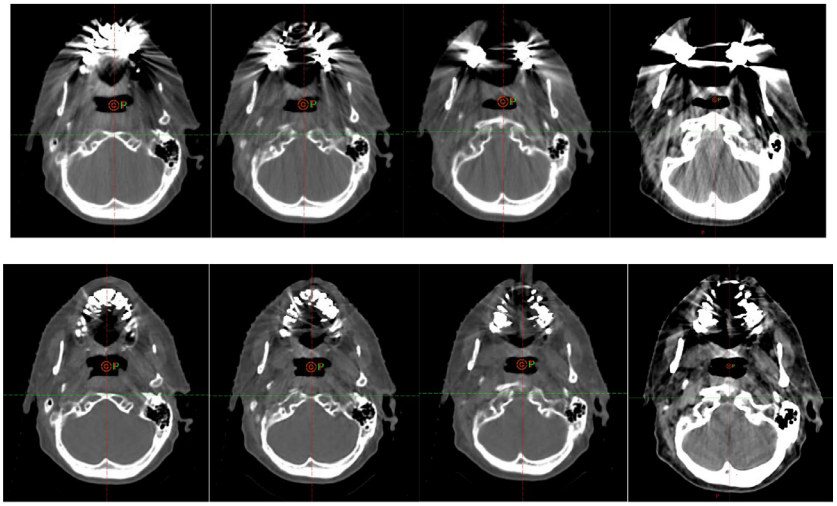

(B)

Figure 3 Comparison of simulation-computed tomography (CT) and HyperSight cone beam (CB) CT on patients with dental filling. (A) The top figures were fan-beam Siemens simulation-CT with metal artifact reduction, and the bottom figures were HyperSight CBCT with iCBCT MAR reconstruction. (B) The top figures were fan-beam GE simulation-CT (without metal artifact reduction), and the bottom figures were HyperSight CBCT with iCBCT MAR reconstruction. For each set of images, the first 3 images were displayed at a window width of 800/-400 HU, and the fourth image at 225/-125 HU.
Abbreviations: HU = Hounsfield unit.

2. For tumor motion amplitude of ± 5 mm and slower motion cycle (6-12 seconds), the tumor position agreement was observed to be highly dependent on the motion phase during CBCT acquisition.

    - If the CBCT acquisition time included both inhalation peak and exhalation valley, the agreement between the center of the tumor on HyperSight CBCT and the center of ITV position on the AIP reference image was observed.
    - If the CBCT acquisition time includes only the inhalation or exhalation phase, a tumor position misalignment was observed.

    Figure 1C shows the ITV alignment of ± 5 mm tumor motion amplitude in a 12-second motion cycle rate, with the CBCT acquisition time encompassing only the inhalation phase. The tumor position for CBCT was observed to lie on the superior edge of the contoured ITV (5 mm tumor center misalignment). The tumor shape shown on CBCT was a sphere, similar to the central portion of the ITV on AIP.
3. For tumor motion amplitudes exceeding ± 5 mm with a motion cycle ≤ 6 seconds, the CBCT acquisition time includes both inhalation and exhalation phases. In those cases, the center of the contoured ITV matched the central portion of the motion blur but there was also an area superior and inferior within the motion blur that was not contained within the contoured ITV (caused by motion > ± 5 mm), as shown

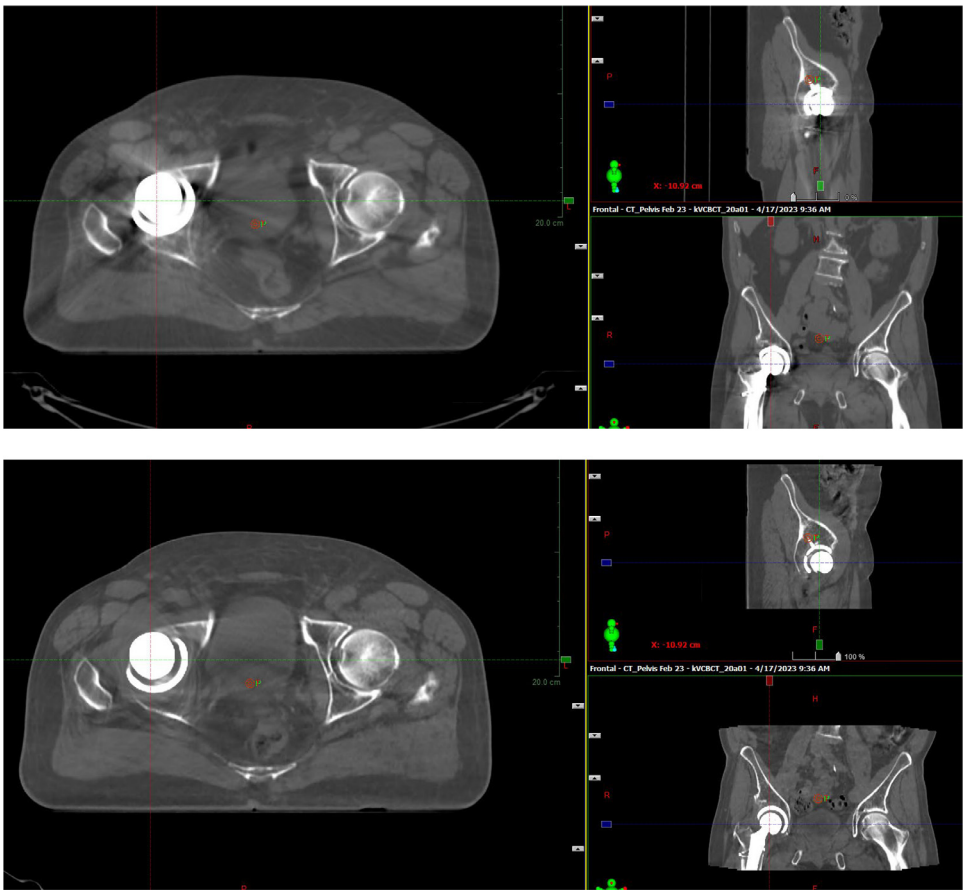

Figure 4 Comparison of simulation-computed tomography (CT) and HyperSight cone-beam (CB) CT on a patient with a prosthesis. The top figures were fan-beam GE simulation-CT and the bottom figures were HyperSight CBCT with iCBCT MAR reconstruction.

in Fig. 1D. The tumor shape shown on CBCT was a motion blur and was different from the ITV on AIP.

4. For tumor motion amplitude exceeding ± 5 mm and motion period exceeding 6 seconds, the tumor position agreement was observed to be highly dependent on the motion phase during CBCT acquisition.
   - If the CBCT acquisition time included both inhalation peak and exhalation valley, the agreement between the center of the tumor on HyperSight CBCT and the center of ITV position on the AIP reference image was observed.
   - If the CBCT acquisition time included only the inhalation or exhalation phase, tumor position misalignment was observed.

   Figure 1E shows the ITV alignment for 3 different scenarios:

   - The top CBCT shows the ITV alignment of ± 10 mm tumor motion amplitude with a 12-second motion cycle rate, and CBCT acquisition time encompasses only the inhalation phase. The tumor position for CBCT was observed to lie on the superior portion of the contoured ITV, and a part of the tumor was outside the superior edge of the contoured ITV (caused by motion > ± 5 mm, ~1 cm tumor center misalignment). The tumor shape shown on CBCT was a sphere, similar to the central portion of the ITV on AIP.
   - The middle CBCT shows the ITV alignment of ± 10 mm tumor motion amplitude with an 11-second motion cycle rate, and CBCT acquisition time included both inhalation peak and exhalation valley. The central portion of the motion blur and the center of the contoured ITV agreement were observed, and part of the motion blur was outside both the superior and inferior edges of the contoured ITV. The tumor shape shown on CBCT was a motion blur and was different from the ITV on AIP.
   - The bottom CBCT shows the ITV alignment of ± 10 mm tumor motion amplitude with a 10-second motion cycle rate, and CBCT acquisition time encompassed only the exhalation phase plus 1-second onset of inhalation. The tumor position for CBCT was observed to lie on the inferior portion of the contoured ITV, and a part of the tumor was

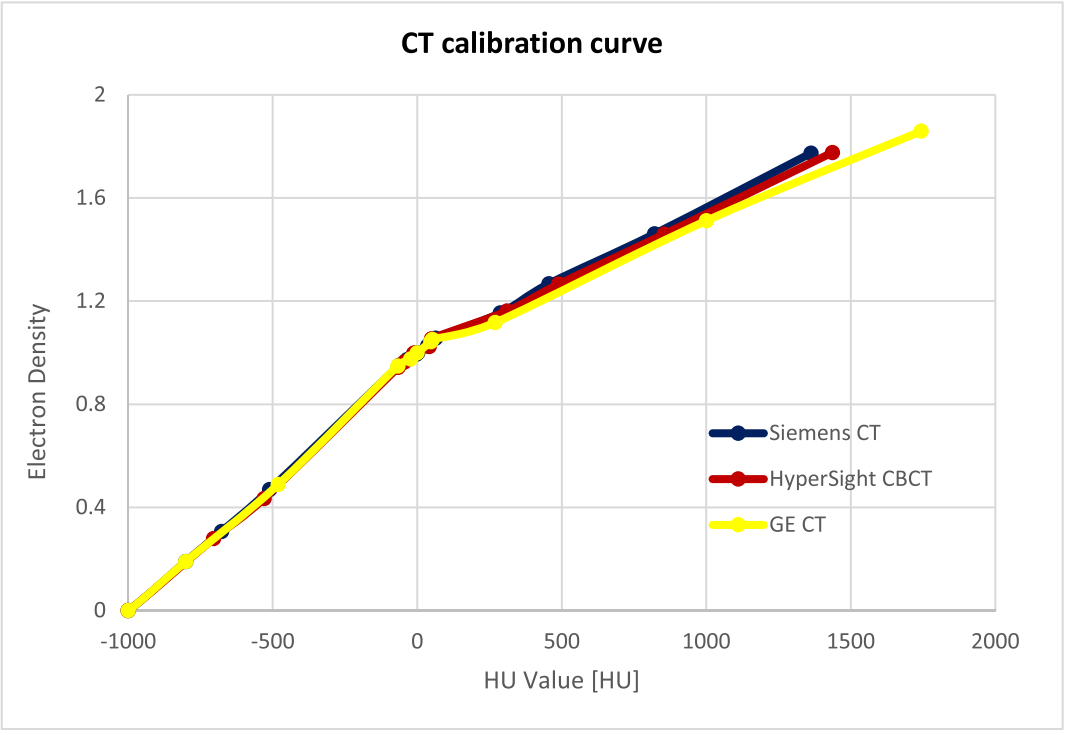

Figure 5 HU value versus electron density comparison among GE simulation-computed tomography (CT), Simens simulation-CT, and HyperSight CBCT.
Abbreviations: CBCT = cone-beam computed tomography; HU = Hounsfield unit.

outside the inferior edge of the contoured ITV (caused by motion > ± 5 mm). The tumor shape shown on CBCT was a sphere, similar to the central portion of the ITV on AIP.

Some image quality improvement opportunities of HyperSight CBCT were observed in this evaluation. Figure 6 shows 2 examples of CBCT image artifacts. The treatment site for the left patient was the esophagus, and the CBCT scan parameters were 125 kV and 651 mAs. The treatment site for the right patient was the pancreas, and the CBCT scan parameters were 125 kV and 773 mAs.

Discussion

In this evaluation, significant improvement of image contrast, HU constancy, and noise level on HyperSight CBCT over traditional CBCT was observed for scatter correction and metal artifact reduction reconstruction methods with 125 and 140 kV settings. The image quality of these CBCTs was within the AAPM TG142 specifications[28-30] for CBCT and within the ± 5 HU constancy and accuracy of water for CT simulator criteria in AAPM TG 66 and Report No. 39.[31,32] The HU uniformity of these HyperSight CBCTs was within 15 HU, slightly higher than the ± 5 HU criteria in AAPM TG66 for the CT simulator. With similar image contrast achieved, HU constancy and noise level for these HyperSight CBCTs were slightly superior to Siemens simulation-CT.

In our study, rigorous image quality assessments were performed on a commonly used phantom (Catphan) rather than real patients. This approach eliminates anatomical variations among different CBCT/CT scans of patients providing a more robust analysis and consistent ground truth.

Robar et al[14] performed an image quality comparison among HyperSight, TrueBeam, and simulation-CT in their clinical study on patient scans. Regions of interest were manually picked among three different scans on similar anatomic locations, and then image artifacts, signal-to-noise ratio, and HU differences were compared. Similar results of significant artifact reduction on HyperSight CBCT compared with TrueBeam CBCT and comparable image artifacts between HyperSight CBCT and fan-beam simulation-CT were shown in patients.

The visual comparison of patient scans in our study showed significantly improved image quality of HyperSight CBCT compared with TrueBeam CBCT and comparable performance of metal artifact reduction between HyperSight CBCT and Siemens simulation-CT. The improved HyperSight CBCT image quality enables clearer visualization of patient anatomy for target and structure alignments, thus facilitating the efficiency and accuracy of daily IGRT image registration and offering the potential for online and offline adaptive RT. The effectiveness of

Table 3 HU consistency for HyperSight CBCT. The top table is for 125 kV CBCT, and the bottom table is for 140 kV CBCT

125 kV		Catphan position							
Material	**Catphan HU**	**Center**	**10 cm superior**	**10 cm inferior**	**10 cm up**	**10 cm down**	**10 cm left**	**10 cm right**	**Max diff.**
Air	−1046:−986	−1000	−1000	−994	−1000	−1000	−1000	−985	6
PMP	−220: −172	−197	−190	−192	−188	−191	−190	−176	21
LDPE	−121:−87	−105	−99	−112	−92	−92	−111	−93	20
Polystyrene	−65:−29	−50	−47	−54	−56	−44	−48	−33	23
Acrylic	92:137	109	108	102	109	112	121	109	19
Delrin	344:387	335	340	326	349	329	338	334	23
Bone 50%	667:783	663	671	635	625	643	674	576	98
Bone 20%	211:263	215	227	206	221	197	204	217	30
Teflon	941:1060	939	939	914	916	934	932	933	25
140 kV		**Catphan position**							
Material	**Catphan HU**	**Center**	**10 cm superior**	**10 cm inferior**	**10 cm up**	**10 cm down**	**10 cm left**	**10 cm right**	**Max diff.**
Air	−1046:−986	−999	−1000	−999	−1000	−1000	−1000	−986	14
PMP	−220: −172	−188	−187	−191	−179	−189	−192	−174	18
LDPE	−121:−87	−96	−94	−107	−84	−93	−107	−88	23
Polystyrene	−65:−29	−44	−45	−52	−51	−43	−46	−35	17
Acrylic	92:137	118	113	102	111	110	115	114	16
Delrin	344:387	346	344	331	358	338	340	338	27
Bone 50%	667:783	644	646	614	598	621	648	558	90
Bone 20%	211:263	214	216	196	216	189	187	205	29
Teflon	941:1060	940	938	911	930	938	930	926	29

Abbreviations: CT = computed tomography; CBCT = cone-beam computed tomography; HU = Hounsfield unit.

Table 4 HU consistency for Siemens simulation-CT scans. The top table is for 120 kV, and the bottom table is for 140 kV

120 kV		Catphan position					
Material	**Catphan HU**	**Center**	**10 cm up**	**9 cm down**	**10 cm left**	**10 cm right**	**Max diff.**
Air	−1046:−986	−979	−976	−978	−966	−968	13
PMP	−220: −172	−176	−172	−177	−173	−174	5
LDPE	−121:−87	−88	−84	−82	−82	−87	6
Polystyrene	−65:−29	−33	−35	−27	−28	−32	8
Acrylic	92:137	122	120	125	123	123	5
Delrin	344:387	345	344	346	347	346	3
Bone 50%	667:783	614	590	608	588	614	26
Bone 20%	211:263	208	207	206	208	201	7
Teflon	941:1060	918	902	919	911	905	17
140 kV		**Catphan position**					
Material	**Catphan HU**	**Center**	**10 cm up**	**9 cm down**	**10 cm left**	**10 cm right**	**Max diff.**
Air	−1046:−986	−980	−977	−978	−966	−968	14
PMP	−220: −172	−171	−167	−171	−163	−168	8
LDPE	−121:−87	−81	−77	−75	−72	−81	9
Polystyrene	−65:−29	−25	−28	−20	−20	−23	8
Acrylic	92:137	128	127	132	129	131	5
Delrin	344:387	348	350	353	348	353	5
Bone 50%	667:783	566	542	556	535	563	31
Bone 20%	211:263	192	190	191	194	187	7
Teflon	941:1060	912	898	909	903	902	14

Abbreviations: CT = computed tomography; CBCT = cone-beam computed tomography; HU = Hounsfield unit; LDPE = low-density polythene; PMP = Polymethylpentene.

metal artifact reduction makes accurate contouring and dose calculation on HyperSight CBCT possible.

HU versus electron density curve agreement between HyperSight CBCT and CT simulators (both GE and Siemens CTs) in this evaluation verified the HU accuracy and enabled the dosimetric accuracy of treatment planning on HyperSight CBCT. Robar et al[14] in their study reported the median HU in HyperSight breath hold imaging was within 15 HU compared with simulation-CT on patients.

An HU variation evaluation when the phantom was placed in the ± 10 cm range in all 3 principal directions

Table 5 Summary of 4-dimensional phantom study

Scenario	Motion amplitude (mm)	Motion cycle (sec)	CBCT acquisition on motion phase	Target center alignment
1	≤ ±5	≤ 6	Any	Aligned
2	± 5	> 6	Including inhalation peak and exhalation valley	Aligned
			Incomplete inhalation peak and exhalation valley	Misaligned
3	> 5	≤ 6	Any	Aligned, with a partial target outside the contoured ITV
4	> 5	> 6	Including inhalation peak and exhalation valley	Aligned, with a partial target outside the contoured ITV
			Incomplete inhalation peak and exhalation valley	Misaligned

Abbreviations: ITV = internal target volume.

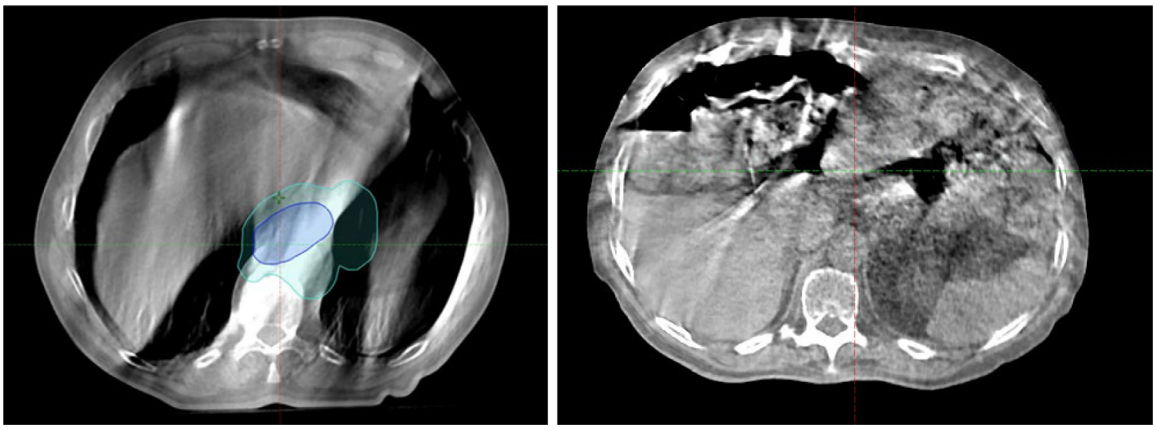

Figure 6 HyperSight CBCT image artifacts. The left figure shows the breathing motion artifacts, and the right figure shows artifacts caused by air inside the patient.
Abbreviations: CBCT = cone-beam computed tomography.

was performed in our study, which is essential for treatment planning. The HU variation for HyperSight CBCT within ± 10 cm in all 3 principal directions was within 100 HU for bone 50% and 30 HU for materials other than bone (50% and 20%), comparing within 31 HU for bone 50% and 17 HU for materials other than bone for Siemens simulation-CT. Similar HU variation on CBCT was observed by Rong et al[33]. According to Davis et al[34], the range of HU tolerances of 40 HU for soft tissue and of 100 HU for the lung and bone would restrict dose changes to < 1% in the treatment plan, which indicates that the spatial HU variation of HyperSight is appropriate for treatment planning.

A typical Varian C-arm 3D CBCT acquisition time is between 40 and 60 seconds, and like helical CT, C-arm 3D CBCT is the image of an average over multiple respiratory cycles. For IGRT image registration purposes, either a maximum intensity projection (MIP) derived from 4DCT or AIP is typically used as a reference image.[35-37] AIP image was recommended as the reference over MIP image for free-breathing CBCT target matching in literature.[36,38] In our 4D lung phantom study, the AIP image was used as a reference.

One of the main differences between C-arm CBCT and HyperSight CBCT is the scan acquisition time. C-arm CBCT is typically an average image over 10 respiratory cycles, but rapid HyperSight CBCT is only average over 1 to 1.5 respiratory cycles. The rapid acquisition is more sensitive to interfractional and intrafractional tumor alignment discrepancies on free-breathing CBCT scans of moving targets. In our study, image registration was performed based on the entire phantom alignment; therefore, the center of the tumor on CBCT should lie on the center of the contoured ITV. Both tumor shape and tumor alignment discrepancies on CBCT scans were observed in this study. The tumor shapes shown on CBCT scans differed from a solid sphere (Fig. 1C, E top and bottom) to different sizes of motion blur (Fig. 1D, E middle), depending on the combination of tumor motion amplitude, motion cycle rate, and motion phase during CBCT acquisition. The significant tumor misalignment was shown on the combination of slower motion cycle rate and CBCT acquired only on inhalation or exhalation phase. Those tumor alignments are the misrepresentations of the center of tumor position. If the IGRT shifts were made based on those alignments, the tumor coverage would be compromised. The results of tumor alignment discrepancy of CBCT with moving target in this study agreed with the published data.[24,36,39] A slow CBCT (40-60 seconds) scan is normally an average image over 10 respiratory cycles; therefore, the agreement between the centers of motion blur with the contoured ITV should be observed in the ideal sinusoidal tumor motion phantom. In July 2023, Varian released an upgraded version of Halcyon (4.0 MR1), which enables a 59.6-second slow HyperSight CBCT scan. This protocol is recommended to be used for scanning moving targets.

For accurate CBCT alignments, it is critical to include the inhalation peak and exhalation valley in the CBCT acquisition. To be able to treat moving targets accurately, various technologies are available for motion monitoring during radiation treatment. It is crucial for the clinic to include the real-time monitoring device in the Halcyon vault before considering treating a moving target such as the lung. The evaluation of respiratory motion and rate can facilitate the selection between rapid and slow HyperSight CBCT. For slower breathers, if rapid CBCT acquisition can't encompass the inhalation peak and exhalation valley, slow HyperSight CBCT is required. The clinical team should design a proper workflow to correlate the CBCT acquisition with the respiratory cycle and use the information to determine the most appropriate CBCT protocol for accurate treatment delivery.

The larger tumor motion amplitude exceeding ± 5 mm of CBCT was tested in this study to simulate the

interfractional and intrafractional tumor motion variations, which have been clinically observed on real patients frequently. Tumor motion of real patients is rarely perfectly sinusoidal; therefore, the uncertainty of tumor location of real patients may be increased and more complicated compared to this phantom study.

It is clinically critical to monitor patient respiratory motion during rapid HyperSight CBCT acquisition, both on motion amplitude and motion cycle rate. If the patient's respiratory motion amplitude and/or motion cycle rate are different from simulation-CT, a possible nonreliable CBCT registration could happen. Surface-guided RT systems are ideal for patient interfractional and intrafractional respiratory motion monitoring. The rapid CBCT also facilitates the breath-hold scan acquisition, which eliminates the need for ITV. Robar et al[14] performed all their patient CBCT scans with the breath-hold technique. Further investigation of the HyperSight CBCT scan with the surface-guided breath-hold technique would have great clinical significance.

Regarding the HyperSight CBCT artifacts, the left image of Fig. 6 shows the breathing motion artifacts. One possible solution is to scan CBCT with breath-hold for tumors in the lung/diaphragm area. The right image shows artifacts caused by air inside the patient. A future improvement of the reconstruction algorithm could hopefully resolve the issue.

Conclusions

This image quality evaluation shows significant image improvement of HyperSight CBCT over conventional CBCT on image contrast, HU constancy, and noise level with scatter correction and metal artifact reduction reconstruction methods for 125 and 140 kV settings. HyperSight CBCT has a similar image quality to fan-beam simulation-CT and shows the potential application for treatment planning. The improved HyperSight CBCT image quality facilitates the efficiency and accuracy of daily IGRT image registration. The effectiveness of metal artifact reduction makes accurate contouring and dose calculation on HyperSight CBCT possible. The rapid acquisition of HyperSight free-breathing CBCT scans showed both tumor shape and tumor alignment discrepancies on CBCT scans of moving targets, depending on the motion amplitude, motion speed, and motion phase during CBCT acquisition. Careful considerations of patient respiratory motion monitoring and target matching are highly recommended.

Disclosures

The authors declare that they have no known competing financial interests or personal relationships that could have appeared to influence the work reported in this paper.

Acknowledgments

Hui Zhao was responsible for statistical analysis.

References

1. Deng L, Zhang M, Wang J, Huang S, Yang X. Improving cone-beam CT quality using a cycle-residual connection with a dilated convolution-consistent generative adversarial network. *Phys Med Biol*. 2022:67.
2. Trapp P, Maier J, Susenburger M, Sawall S, Kachelrieß M. Empirical scatter correction: CBCT scatter artifact reduction without prior information. *Med Phys*. 2022;49:4566-4584.
3. Zhang Y, Zhang L, Zhu XR, Lee AK, Chambers M, Dong L. Reducing metal artifacts in cone-beam CT images by preprocessing projection data. *Int J Radiat Oncol Biol Phys*. 2007;67:924-932.
4. Deng L, Ji Y, Huang S, Yang X, Wang J. Synthetic CT generation from CBCT using double-chain-CycleGAN. *Comput Biol Med*. 2023;161:106889.
5. Rusanov B, Hassan GM, Reynolds M, et al. Deep learning methods for enhancing cone-beam CT image quality toward adaptive radiation therapy: A systematic review. *Med Phys*. 2022 Sep;49:6019-6054.
6. Gardner SJ, Mao W, Liu C, et al. Improvements in CBCT image quality using a novel iterative reconstruction algorithm: a clinical evaluation. *Adv Radiat Oncol*. 2019;4:390-400.
7. Jin JY, Ren L, Liu Q, et al. Combining scatter reduction and correction to improve image quality in cone-beam computed tomography (CBCT). *Med Phys*. 2010;37:5634-5644.
8. Men K, Dai J, Chen X, Li M, Zhang K, Huang P. Dual-energy imaging method to improve the image quality and the accuracy of dose calculation for cone-beam computed tomography. *Phys Med*. 2017;36:110-118.
9. Wang H, Liu X, Kong L, et al. Improving CBCT image quality to the CT level using RegGAN in esophageal cancer adaptive RT. *Strahlenther Onkol*. 2023;199:485-497.
10. Imae T, Kaji S, Kida S, et al. [Improvement in image quality of CBCT during treatment by cycle generative adversarial network]. *Nihon Hoshasen Gijutsu Gakkai Zasshi*. 2020;76:1173-1184. Japanese.
11. Lim R, Penoncello GP, Hobbis D, Harrington DP, Rong Y. Technical note: Characterization of novel iterative reconstructed cone beam CT images for dose tracking and adaptive RT on L-shape linacs. *Med Phys*. 2022;49:7715-7732.
12. Henke LE, Fischer-Valuck BW, Rudra S, et al. Prospective imaging comparison of anatomic delineation with rapid kV cone beam CT on a novel ring gantry radiotherapy device. *Radiother Oncol*. 2023;178:109428.
13. Cai B, Laugeman E, Mazur TR, et al. Characterization of a prototype rapid kilovoltage x-ray image guidance system designed for a ring shape radiation therapy unit. *Med Phys*. 2019;46:1355-1370.
14. Robar JL, Cherpak A, MacDonald RL, et al. Novel technology allowing cone beam computed tomography in 6 seconds: a patient study of comparative image quality. *Pract Radiat Oncol*. 2024;14:277-286.
15. Siva S, Chesson B, Aarons Y, et al. Implementation of a lung radiosurgery program: technical considerations and quality assurance in an Australian institution. *J Med Imaging Radiat Oncol*. 2012;56:354-361.
16. Park JC, Park SH, Kim JH, et al. Liver motion during cone beam computed tomography guided stereotactic body radiation therapy. *Med Phys*. 2012;39:6431-6442.

17. Wang Z, Wu QJ, Marks LB, Larrier N, Yin FF. Cone-beam CT localization of internal target volumes for stereotactic body radiotherapy of lung lesions. *Int J Radiat Oncol Biol Phys*. 2007;69:1618-1624.
18. Yeung AR, Li JG, Shi W, et al. Tumor localization using cone-beam CT reduces setup margins in conventionally fractionated radiotherapy for lung tumors. *Int J Radiat Oncol Biol Phys*. 2009;74:1100-1107.
19. Cao X, Liu M, Zhai F, et al. Comparative evaluation of image registration methods with different interest regions in lung cancer radiotherapy. *BMC Med Imaging*. 2019;19:100.
20. Padmanaban S, Boopathy R, Kunjithapatham B, Sukumar P, Nagarajan V. The effects of target motion in kV-CBCT imaging. *Pol J Radiol*. 2010;75:61-66.
21. Vergalasova I, Maurer J, Yin FF. Potential underestimation of the internal target volume (ITV) from free-breathing CBCT. *Med Phys*. 2011;38:4689-4699.
22. Lens E, van der Horst A, Kroon PS, et al. Differences in respiratory-induced pancreatic tumor motion between 4D treatment planning CT and daily cone beam CT, measured using intratumoral fiducials. *Acta Oncol*. 2014;53:1257-1264.
23. Tan Z, Liu C, Zhou Y, Shen W. Preliminary comparison of the registration effect of 4D-CBCT and 3D-CBCT in image-guided radiotherapy of Stage IA non-small-cell lung cancer. *J Radiat Res*. 2017;58:854-861.
24. Kamomae T, Monzen H, Nakayama S, et al. Accuracy of image guidance using free-breathing cone-beam computed tomography for stereotactic lung radiotherapy. *PLoS One*. 2015;10:e0126152.
25. Tanyi JA, Fuss M, Varchena V, Lancaster JL, Salter BJ. Phantom investigation of 3D motion-dependent volume aliasing during CT simulation for radiation therapy planning. *Radiat Oncol*. 2007;2:10.
26. Goodenough DJ, Weaver KE. Factors related to low contrast resolution in CT scanners. *Comput Radiol*. 1984;8:297-308.
27. Advanced Electron Density Phantom. Tissue-equivalent CT-to-electron density calibration. Accessed Feb 9, 2023. https://www.sunnuclear.com/products/advanced-electron-density-phantom.
28. Klein EE, Hanley J, Bayouth J, et al. Task Group 142 report: quality assurance of medical accelerators. *Med Phys*. 2009;36:4197-4212.
29. Taneja S, Barbee DL, Rea AJ, Malin M. CBCT image quality QA: Establishing a quantitative program. *J Appl Clin Med Phys*. 2020;21:215-225.
30. Manger RP, Pawlicki T, Hoisak J, Kim GY. Technical note: assessing the performance of monthly CBCT image quality QA. *Med Phys*. 2019;46:2575-2579.
31. Mutic S, Palta JR, Butker EK. Quality assurance for computed-tomography simulators and the computed-tomography-simulation process: report of the AAPM Radiation Therapy Committee Task Group No. 66. *Med Phys*. 2003;30:2762-2792.
32. Torfs K, Vignero J, Lemmens K, et al. Specification and Acceptance Testing of Computed Tomography Scanners (American Institute of Physics, New York, 1993). Accessed Feb 9, 2023. https://www.aapm.org/pubs/reports/rpt_39.pdf.
33. Rong Y, Smilowitz J, Tewatia D, Tomé WA, Paliwal B. Dose calculation on kV cone beam CT images: an investigation of the Hu-density conversion stability and dose accuracy using the site-specific calibration. *Med Dosim*. 2010;35:195-207.
34. Davis AT, Palmer AL, Nisbet A. Can CT scan protocols used for radiotherapy treatment planning be adjusted to optimize image quality and patient dose? A systematic review. *Br J Radiol*. 2017;90:20160406.
35. Song JY, Nam TK, Ahn SJ, Chung WK, Yoon MS, Nah BS. Respiratory motional effect on cone-beam CT in lung radiation surgery. *Med Dosim*. 2009;34:117-125.
36. Li X, Li T, Yorke E, et al. Effects of irregular respiratory motion on the positioning accuracy of moving target with free breathing cone-beam computerized tomography. *Int J Med Phys Clin Eng Radiat Oncol*. 2018;7:173-183.
37. Wang L, Chen X, Lin MH, et al. Evaluation of the cone beam CT for internal target volume localization in lung stereotactic radiotherapy in comparison with 4D MIP images. *Med Phys*. 2013;40:111709.
38. Shirai K, Nishiyama K, Katsuda T, et al. Phantom and clinical study of differences in cone beam computed tomographic registration when aligned to maximum and average intensity projection. *Int J Radiat Oncol Biol Phys*. 2014;88:189-194.
39. Blake SJ, Dillon O, Byrne HL, O'Brien RT. Thoracic motion-compensated cone-beam computed tomography in under 20 seconds on a fast-rotating linac: a simulation study. *J Appl Clin Med Phys*. 2023;24:e13909.